Mechanical Systems and Signal Processing 184 (2023) 109680

Contents lists available at ScienceDirect

Mechanical Systems and Signal Processing

journal homepage: www.elsevier.com/locate/ymssp

Modelling and identifying a pressurised dilatant sand to be used as a smart damping material

Jacek M. Bajkowski [a], Bartłomiej Dyniewicz [b], Jerzy Bajkowski [c], Czesław I. Bajer [b,*]

[a] Faculty of Production Engineering, Warsaw University of Technology, Narbutta 85, 02-524 Warsaw, Poland
[b] Institute of Fundamental Technological Research, Polish Academy of Sciences, Pawińskiego 5b, 02-106 Warsaw, Poland
[c] Faculty of Aviation, Polish Air Force University, Dywizjonu 303 35, 08-521 Dęblin, Poland

ARTICLE INFO

Communicated by J. Noël

Keywords:
Granular material
Damping
Dilatant sand
Identification
Control

ABSTRACT

An experimental and modelling study of the properties of a prototype layered beam with a core made of a non-Newtonian sand mixture is presented. The non-typical dilatant sand was covered with an elastic envelope that restricted its movement, which allowed us to pressurise the grains by evacuating the air from within the cover. By applying controlled underpressure, the compressed sand grains become jammed, which resulted in an increased stiffness and damping. This gives the possibility to attenuate vibrations of a cantilever in an adaptive manner. The experiment was performed for free vibrations and prescribed sinusoidal base motion, to demonstrate the possibility of tuning material parameters in a vast range. The experimental amplitude, frequency and damping capacity of the kinetic sand are discussed. An analytical model is proposed to verify how many parameters are necessary to describe the material behaviour. Based on the experimental results, a parameter identification of a custom rheological model is performed and practical simplifications reducing complexity of the problem are elaborated. The performed parameter identification is indispensable for the further development of potential control strategies for effective vibration abatement of dynamic systems using such types of alternative smart materials.

1. Introduction

Many different types of smart materials (e.g., piezoelectrics, magnetorheological or electrorheological fluids or elastomers) are being researched as possible solutions in semi-active vibration reduction systems. Although they are rarely categorised as "smart", the bulk granular materials that we consider in this paper appear to be another promising solution for reducing unwanted vibrations thanks to their non-typical dissipating properties. Usually, it is not possible to adjust the dissipation of bulk material because it is used passively by placing granules in a container attached to a vibrating system or fitting them into structural voids [1–3].

Although cost effective and robust, the impact damper's parameters cannot be adjusted once it is setup. Consequently, the passive attenuation becomes ineffective when dynamics or disturbances vary with time. The granules in a typical particle impactor are free to move and collide, similar to a gas-like state. In contrast, the solution that we describe in this paper explores the properties of a granular media in a quasi-solid phase, which is also described as a jammed state.

A prototype beam with a dissipating core with jammed spherical granules was previously introduced in [4], along with a simplified study of the system's parameters. It was mentioned in this study that the issue of modelling the structure is open for development, taking into consideration additional parameters to allow us to describe the properties of bulk material globally. The

* Corresponding author.
E-mail address: cbajer@ippt.pan.pl (C.I. Bajer).

https://doi.org/10.1016/j.ymssp.2022.109680
Received 13 May 2021; Received in revised form 20 May 2022; Accepted 8 August 2022
Available online 26 August 2022

present work, describes this development by taking advantage of improved beam construction, including a modified concept of the adaptive damping core, unique material selection and complex parameter identification.

Instead of simply using plastic spherical granules, a non-Newtonian sand suspension was used to fill the core of a prototype sandwich beam. Moreover, the sand was covered with a special elastic envelope to confine the movement of the sand grains, preventing spilling and allowing us to pressurise the core by evacuating the air from the envelope. Unlike a typical granular impactor, in our setup the sand grains remain in constant contact thanks to the envelope. Thus, the non-conservative interactions among the jammed particles can be weakened or intensified, depending on the level of material compression, which can be adjusted pneumatically. A study based on experiments concerning free and forced vibrations is performed for different underpressure values.

This paper aims to study the damping effectiveness of special sand by obtaining a set of parameters to allow us to model the beam system. In the first stage, a mathematical model of a layered beam with a smart core was created and the parameters affecting its dynamics were investigated. Elaborating the simplified model that exhibits properties of a more complex reference sandwich beam model enabled us to determine the rheological type of structural behaviour. However, the identification is difficult because dilatant sand exhibits properties that differ significantly from the properties of continuous Newtonian materials and depend on underpressure. The scale of the task is therefore growing and simplification is necessary. A rheological elastic with the hardening-viscoplastic model was considered to find the minimum number of parameters to describe the system with a satisfying accuracy. Additional identification revealed that in the case of a 12-parameter model, some of the parameters become equal to zero and may be removed, while other may be assumed to be constant. For practical reasons, the simplified rheological model using a set of nine surrogate parameters is sufficient to adequately represent the dynamics of a sandwich beam with pressurised kinetic sand used as a damping material. Moreover, the number of pressure-dependent variables can be significantly reduced, which is promising for further optimisation studies because the computational cost may be significantly decreased.

2. Adjustable granular damping

Typically, passive impact dampers are designed as artificial containers with granules colliding inside an enclosure that is attached to the main vibrating system [5–7]. When the granules vibrate, the energy is dissipated due to complex, non-conservative interactions combining friction, slips, exchange of momentum, particle reorientation, local deformations, and so on [8–10]. A complete survey providing an overview of various mechanisms accompanying granular dissipation in different types of impact dampers is presented in [11].

Implementing the concept of semi-active damping requires the possibility of mechanically alternating the material's parameters according to some control signal. Magnetorheological and electrorheological fluids or elastomers achieve this by modifying a magnetic field [12,13], piezoelectrics use electric signals [14], while shape-memory alloys undergo thermal and mechanical control [15]. In contrast, granular dampers usually lack the possibility of semi-active control because they operate in a passive regime.

To overcome this issue, a container filled with bulk granules can be designed in such a way to allow the ensemble to be compressed [16]. The concept of a container with adjustable geometry has been explored in [17], where granules were placed inside a rigid cylinder and a special o-ring allowed the pre-compression to be adjusted. In [18], the granule-filled container geometry was morphed using a shape-memory alloy. In [19], soft encapsulation was used to increase the rigidity of a granular ensemble to make a flexible endoscope guide with controllable rigidity, while in [20] it was used to make a soft robotic gripper. In [21], a soft sleeve filled with granules was used to cover a steel beam. Pneumatic systems were recently used to maintain pressure on the boundaries of the cellular damping structure in [22].

A confining pressure preserves the particle arrangement and enhances the rigidity of an externally bounded granular structure. Therefore, it influences the level of energy dissipation, depending primarily on the phase of granular matter. The granular structure considered in this paper exploits reversible phase transition, from fluid-like to semi-solid state. This change of state is called the jamming transition. The driving mechanism causing dissipation in the jammed state is complex. The influence of friction and slips among particles, and between the particles and the envelope was covered in [23,24]. Particle intrusion and local deformations were discussed in [25], while particle hopping was discussed in [26]. Although the non-trivial properties of granular materials in the jammed state has been the subject of many studies, very few papers have described solutions exploring this phenomenon for effective vibration damping.

Our approach to modelling the non-typical sand mixture is far from the advanced modelling of sand/soil systems considered in geomechanics. In [27] authors proposed an equivalent linear method of analysis with a set of frequency-dependent moduli and damping of inelastic soil. In [28] a generalised three-dimensional nonlinear viscoelastic model for sand system under seismic excitation was employed. Groholski et al. proposed a general quadratic model with nonlinear behaviour controlled by a shear strain-dependent curve-fitting function [29]. In [30] authors developed a modified Bouc–Wen (B–W) model to capture the cyclic stress–strain hysteresis soil. However, identifying a large number of parameters of the B–W model is problematic. In [31] authors successfully used particle swarm optimisation to identify parameters describing the asymmetric hysteresis of the B–W of sand. In [32] a genetic algorithm was used for the identification of a granular system. Our research aimed at finding a model that could represent the behaviour of the sand/envelope/cantilever system globally. Such a model could be adapted to design an adaptive control system since fewer parameters promote robust control.

Fig. 1. Mixture of a 98% of fine sand and 2% coating called kinetic sand.

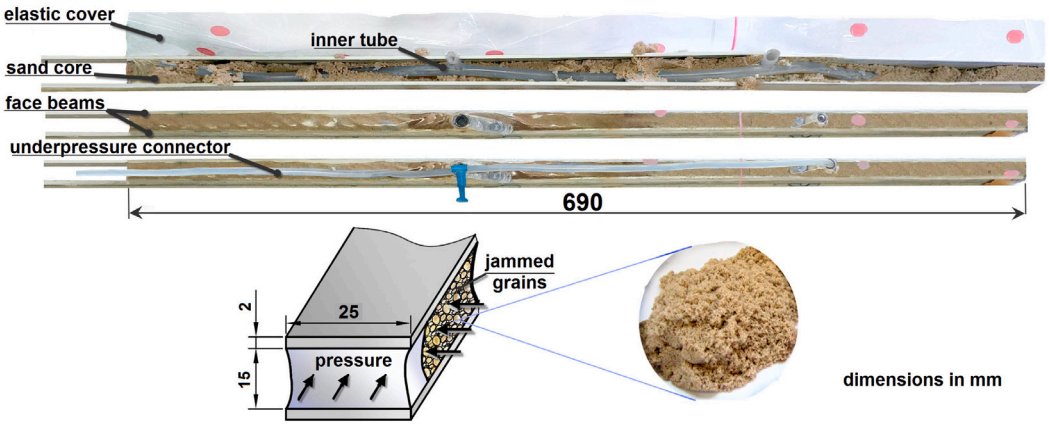

Fig. 2. Design of the layered beam with a sand-filled core subjected to underpressure.

3. Materials, methods and experimental setup

3.1. Layered beam construction

The granular material examined in this article was a suspension of 98% fine natural sand coated with a thick layer of active linear silicone polymer. The remaining 2% of non-toxic polydimethylsiloxane dimethicone 500 was used as a polymer. The coating was viscous and hydrophobic, which helped the sand grains to agglomerate and stuck together. The density of the sand suspension was 1525 kg/m^3. The unique properties of this non-Newtonian suspension allowed it to be easily shaped and made it easy to be moulded without making a mess because the grains stuck together (Fig. 1). Experiments were conducted at an ambient temperature of 20–22 °C and relative humidity of 40%–45%. In contrast to standard sand, the hydrophobic silicone coating made the mixture repel moisture, so the influence of humidity on the results was marginal. Over a longer time, or if disturbed, volumes formed of such sand will collapse. A similarly composed mixture is available as an educational toy, known as kinetic sand.

The sandwich structure proposed in this paper was based on the idea of placing the dilatant sand grains in a thin, airtight, elastic envelope that merged two beams. The considered sandwich cantilever consisted of two, 690 mm long, parallel aluminium strips with a Young's modulus $E = 69$ GPa. The rectangular cross-section of a single strip was 25×2 mm and the strips were separated by 15 mm. A 0.8 mm thin layer of PVC foil was used as an envelope covering the space between the strips and preventing the sand composition from spilling. The total weight of the sandwich beam with a filled core was 0.610 kg. Two pressure connectors were sealed along the envelope. To ensure uniform underpressure distribution inside the envelope, a hollow, perforated elastic tube was placed inside the core and attached to the connectors. The design of the specimen and principle of operation are presented in Fig. 2.

3.2. Laboratory stand

The experimental test stand consisted of a massive clamp, fixed to the sandwich cantilever in a horizontal orientation. A steel spacer separating the outer face layers was placed in the fixture section, to ensure a uniform distribution of the clamping pressure. Three laser sensors with dedicated amplifiers (type ZS-LD and ZX2-LD by Omron and type Microtrak II by MTI Instruments) were used to measure transverse displacement at the beam's tip, and then at 2/3 and 1/3 of the total length l. The recorded displacement

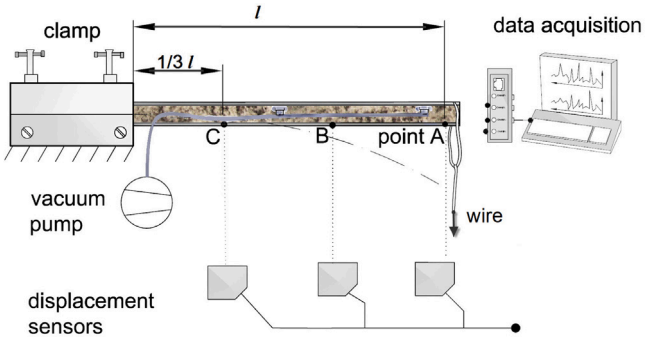

Fig. 3. Scheme of the experimental stand for the free vibration test.

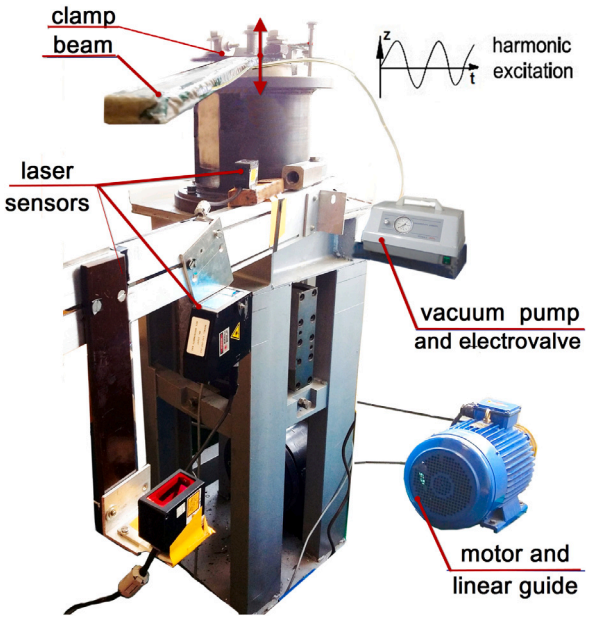

Fig. 4. Photo of the experimental stand used during forced vibration tests.

signals were named A, B and C, respectively. Each of the sensors had different operating parameters but the measurement resolution was not less than 20 μm at a 1 kHz sampling frequency, which was far beyond the required parameters. A vacuum pump was connected to a solenoid valve, while an Omron E8CC digital underpressure sensor monitored the vacuum level. Maintaining a leak-proof and robust pressure control system was essential because underpressure directly influences performance. A 16-bit National Instruments 6210 data acquisition card was used to acquire the results. Two different experimental configurations were setup because separate experiments for free and forced vibrations were conducted.

In the free vibrations test (Fig. 3), the cantilever was fixed horizontally and a wire was attached to the tip to deflect it initially. Underpressure was set individually before deflecting the beam at a selected level, ranging from 0 to 0.08 MPa. When the wire was released, the free response of the beam was recorded.

In a forced vibrations test setup (Fig. 4), the horizontal beam fixing is allowed to move transversely up and down, along the vertical axis. An electric motor with a gear and linear guide allowed the manual setting of different excitation frequencies, ranging up to 11 Hz. The peak-to-peak displacement of the fixture was 10 mm due to the mechanical construction of the gear and guide. Laser sensors were used to record the amplitude for different values of underpressure.

4. Experimental results

4.1. Free vibration

The experimental results of the free vibrations were recorded for different initial deflections (15, 30, 45, 60 and 90 mm) and different underpressure values (0, 0.005, 0.02, 0.04, 0.06 and 0.08 MPa). The combined results of the beam's tip displacement, for

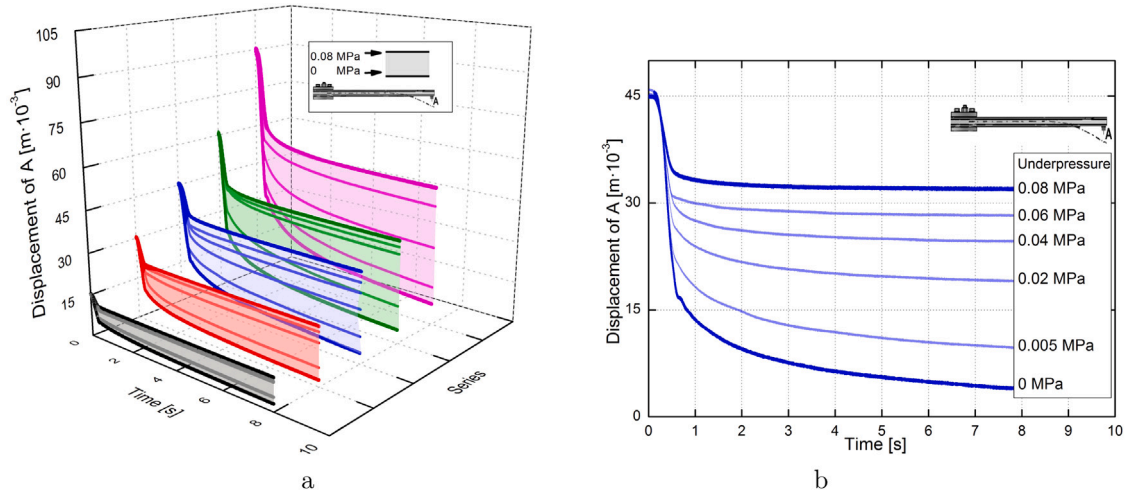

Fig. 5. Displacement of the beam's tip, recorded for different initial excitation and underpressure: (a) collection of results and (b) results for initial deflection of 45 mm.

different initial deflections, are depicted in Fig. 5a. For each series of initial deflections, the top and bottom contour lines of the area represent the response for maximum underpressure (0.08 MPa) and no underpressure (0 MPa), respectively. The remaining lines represent amplitudes over time, for the remaining values of underpressure. Fig. 5b presents the selected group of results obtained after initially deflecting the beam at 45 mm.

It can be seen that increasing underpressure up to 0.08 MPa causes an intense change in the beam's response but this is restricted, as the granular jamming interactions start to gain their maximum potential. This is mainly related to the restriction of the movement of the grains, which cannot be indefinitely compressed, and their relative movement and sliding become much more limited. From the expanded view of the transient response for initial deflection of 45 mm, one sees that the beam is overdamped. After releasing the wire, the energy accumulated in the aluminium strips causes a rapid return towards the non-deflected state. For no underpressure, the deflection amplitude drops from 45 mm to 17 mm in just 0.45 s after the release. Further movement is drastically slowed down because sand dissipation starts to play a significant role. It takes almost 15 s for the beam to approach the non-deflected equilibrium.

Applying underpressure intensifies granular jamming and, thus, core stiffness and damping properties are altered. For the minimum underpressure of 0.005 MPa, the beam needed 26 s to return to a non-deflected state; for 0.02 MPa it took 36 s. When underpressure is increased to 0.04 MPa and further, the beam becomes heavily overdamped and the intensively jammed granules prevent it from returning to the non-deflected state. For 0.08 MPa, the compressed sand core keeps the beam deflected at 32 mm from the equilibrium. The beam basically remains plastically deformed but can be forced to return to the non-deflected state by simply reducing the underpressure by opening the valve or unsealing the envelope. This opens the possibility of dynamically altering the total stiffness and taking advantage of the parametric modification of the structure.

When granular or porous media is used, the responses may differ from test to test. Although our system resembles more of a dense liquid or quasi-solid system because the kinetic sand is mixed with an adhesive and pressurised, the statistical analysis establishes the reliability of the experimental content. All the decay curves were recorded three to five times per single combination of underpressure and initial displacement, to allow a statistical evaluation of the measurements. A meticulous protocol was followed, to ensure that all test runs were repeated for the same conditions. Then, average curves for each combination of deflection and underpressure were calculated. They were used as references to compute and track the standard deviation σ over time, to quantify the repeatability of the results. The standard deviation for initial deflection of 30 mm and 90 mm is presented in Fig. 6. Results for no underpressure and maximum underpressure of 0.08 MPa were presented with bold lines, while the results for the remaining values were omitted for the sake of readability. The standard deviation value was low for all the recorded results, reaching just several millimetres for worst cases. It was observed that the standard deviation peaks in the first second after releasing the beam, and then it stabilises. Generally, higher values of standard deviation were recorded at higher values of underpressure.

4.2. Forced vibrations

Because the beam was overdamped and no oscillatory movement was present in the system, the vibratory movement was forced to reveal damping performance in a dynamic load scenario. We aimed to design a universal constructional element (cantilever, strut, rod or pillar) with an integrated feature of adjustable damping. It would allow adapting the system parameters to the load, e.g. adjusting the stiffness of a traffic signpost to the wind speed. Being aware of the potential exploitation conditions, we tested the low-frequency response with high displacement amplitudes.

The beam was fixed, as shown in Fig. 4, and the fixture was subjected to a prescribed sinusoidal base motion. Fig. 7 presents the results for no underpressure and after jamming the grains with 0.08 MPa underpressure. The harmonic excitation frequency

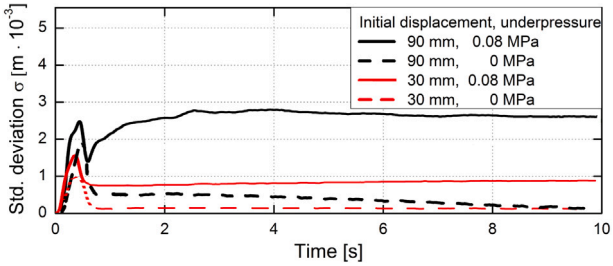

Fig. 6. Standard deviation tracked over time for initial deflection of 30 mm and 90 mm.

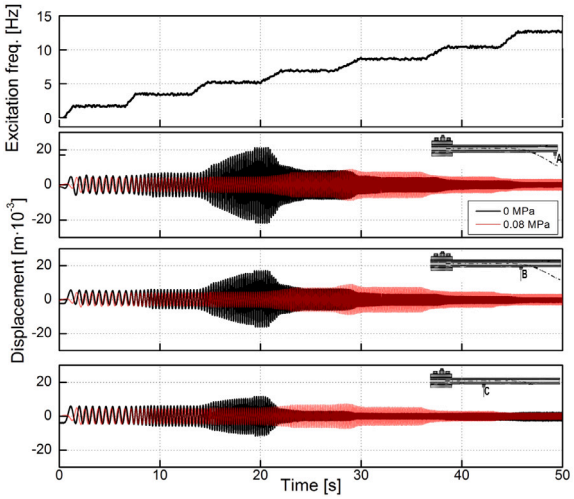

Fig. 7. Comparison of dynamic excitation results for no underpressure and under 0.08 MPa.

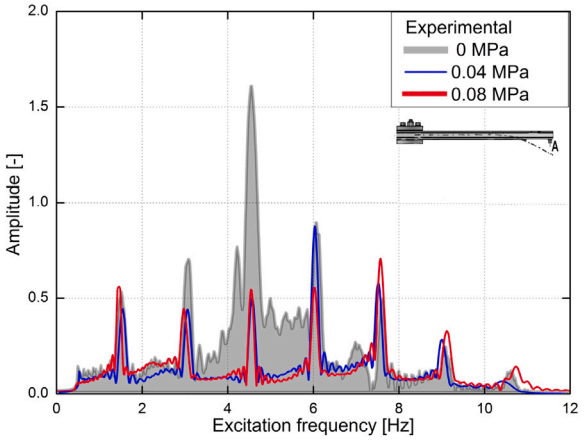

Fig. 8. Experimental results, showing performance of the beam for different excitation frequencies.

was increased in steps. As plotted along the top row, the frequency was constant at each interval, long enough to stabilise transient processes. The lower rows present amplitudes recorded at points A, B, and C.

When the frequency is below 3.5 Hz, the beam replicates the transverse movement of the fixture. After the initial 15 s, when the excitation frequency increases above 3.5 Hz, the beam experiences the first vibration mode and resonance is observed. For no underpressure, the beam reaches resonant vibrations close to 20 s when the frequency reaches 4.56 Hz, resulting in a peak-to-peak displacement of 44 mm at the beam's tip (point A). For underpressure of 0.08 MPa, the resonance is reached after 28 s at the frequency of 6.1 Hz. The displacement reaches a peak-to-peak value of only 12 mm.

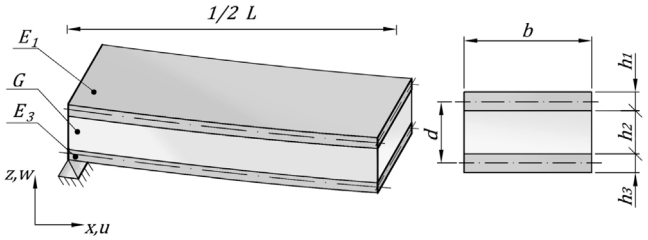

Fig. 9. The three-layered sandwich beam and basic notation.

Fig. 8 compares the amplitudes of the beam's tip for each frequency step and different underpressure values. The unitless amplitude in FFT plots is the relative strength of the harmonic component present in the original signal. When sand is pressurised, the increased stiffness moves the resonance frequency up to higher values, while the increased dissipation results in lower amplitudes. The amplitude at each frequency is always lower when underpressure is applied because the dissipation is intensified.

The results indicate a decent possibility of altering the beam's damping by the underpressure signal. A proper model of the granular structure and identifying of its parameters is necessary for further study of an optimised control system; this should allow us to mitigate the vibrations by alternatively selecting underpressure to achieve maximum damping capacity.

5. Mathematical model of a layered beam

This section aims to present a relatively simple mathematical model of vibration of a three-layer beam with a core filled with dilatant sand to determine how far the system could be simplified. The analytical parameters do not translate directly into the rheological model, and they were derived and identified in a separate procedure. The assumptions of the Mead and Markus model [33] were partially used. The presented equation of motion shows that the mechanical properties of the middle layer can be represented by a small number of phenomenological parameters tuned to the model using the experimentally obtained results.

Instead of a cantilever configuration, a simply supported sandwich beam was considered for mathematical reasons. The mathematical analysis of such a system is much more convenient than in the case of a cantilever beam, while the initial distribution of the bending moment is identical to the half of the simply supported beam.

This assumption is valid in the case of static deformations for point and continuous loads. In free vibrations, the initial static deflection of the beam's tip initiates a motion similar to the first natural mode, which in the case of a cantilever configuration, gradually deviates from the transverse motion of the simply supported beam. In the case of the analysed system, the movement motion is strongly suppressed in the overdamped range, so the displacement differences that appear in both support schemes can be ignored.

The curvatures of both deflection lines are identical. Let us consider a sandwich beam of length L and width b. The thickness of layer i was denoted by h_i. Mass per unit length of the beam was denoted by μ. According to Fig. 9 the transverse displacements in the z direction were denoted by w, while the longitudinal displacements in the x direction of the face-plate i were denoted by u_i. The beam vibrations are induced by initial displacement with a maximum amplitude w_0 and zero initial velocities.

The proposed linear model enables an analytical solution to the given problem. The mathematical model assumes elastic outer layers described by the Young modulus E_i, in which shear strains are neglected. The core is linearly viscoelastic, neglecting longitudinal stresses. Shear was assumed to be constant in the core and described by the Kirchhoff modulus G. Concerning the Mead and Markus model, the shear stresses were supplemented with a damping term according to the Voigt model

$$\tau = G\left[\frac{d}{h_2}\left(\frac{\partial w}{\partial x} + \beta\frac{\partial^2 w}{\partial x \partial t}\right) + \frac{u_1 - u_3}{h_2}\right]. \tag{1}$$

The new parameter β introduces the internal damping in the term describing shear stress in the core. According to the balance of force and balance of strain stress, the system of two conjugated differential equations can be written in the following form

$$\frac{\partial^4 w}{\partial x^4} - gY\left(\frac{\partial^2 w}{\partial x^2} + \beta\frac{\partial^3 w}{\partial x^2 \partial t}\right) + \frac{gE_3h_3d}{D_t}\frac{\partial u_3}{\partial x} + \frac{\mu}{D_t}\frac{\partial^2 w}{\partial t^2} + \frac{c}{D_t}\frac{\partial w}{\partial t} = 0, \tag{2}$$

$$\frac{\partial^2 u_3}{\partial x^2} - \frac{g}{b}u_3 = -\frac{gYD_t}{E_3h_3db}\left(\frac{\partial w}{\partial x} + \beta\frac{\partial^2 w}{\partial x \partial t}\right), \tag{3}$$

where

$$g = \frac{Gb}{h_2}\left(\frac{1}{E_1h_1} + \frac{1}{E_3h_3}\right), \tag{4}$$

$$Y = \frac{d^2}{D_t}\frac{E_1h_1E_3h_3}{E_1h_1 + E_3h_3}. \tag{5}$$

Parameter c is responsible for damping in the entire beam. The distance between face-plates d according to Fig. 9 can be written in the following form

$$d = \frac{1}{2}h_1 + h_2 + \frac{1}{2}h_3. \tag{6}$$

D_t is the total flexural stiffness of the outer layers described, as follows

$$D_t = E_1 I_1 + E_3 I_3, \tag{7}$$

where I_1 and I_3 are the second moment of area of the face-plates. The Eqs. (2) and (3) can be presented in the form of one equation depending only on the transverse displacements w

$$\frac{\partial^6 w}{\partial x^6} - gY\left(\beta\frac{\partial^5 w}{\partial x^4 \partial t} + \frac{\partial^4 w}{\partial x^4}\right) - \frac{g}{b}\frac{\partial^4 w}{\partial x^4} + \frac{\mu}{D_t}\left(\frac{\partial^4 w}{\partial x^2 \partial t^2} - \frac{g}{b}\frac{\partial^2 w}{\partial t^2}\right) + \frac{c}{D_t}\left(\frac{\partial^3 w}{\partial x^2 \partial t} - \frac{g}{b}\frac{\partial w}{\partial t}\right) = 0. \tag{8}$$

To solve the above equation of motion the Fourier transformation was used. The transverse displacement of the sandwich beam in the case of simply supported ends can be written in the following form

$$w(x,t) = \frac{2}{L}\sum_j A_j(t)\sin\lambda_j x, \tag{9}$$

where

$$A_j(t) = \int_0^L w(x,t)\sin\lambda_j x\,\mathrm{d}x. \tag{10}$$

After necessary amendments, Eq. (8) can be transformed into the following form

$$\frac{\mu}{D_t}\left(\lambda_j^2 + \frac{g}{b}\right)\ddot{A}_j(t) + \left(gY\beta\lambda_j^4 + \frac{c}{D_t}\lambda_j^2 + \frac{cg}{D_t b}\right)\dot{A}_j(t) + \lambda_j^4\left(\lambda_j^2 + \frac{g}{b} + gY\right)A_j(t) = 0, \tag{11}$$

where the eigenfunction λ_j according to applied boundary conditions is as follows

$$\lambda_j = \frac{j\pi}{L}. \tag{12}$$

To solve Eq. (11) the Laplace–Carson transformation was taken into account

$$\hat{A}_j(p) = p\int_0^\infty A_j(t)e^{-pt}\,\mathrm{d}t. \tag{13}$$

According to assumed initial conditions the transformation of Eq. (11) can be presented in the following form

$$\begin{aligned}\frac{\mu}{D_t}\left(\lambda_j^2 + \frac{g}{b}\right)\left[p^2\hat{A}_j(p) - p^2 A_j(0)\right] + \left(gY\beta\lambda_j^4 + \frac{c}{D_t}\lambda_j^2 + \frac{cg}{D_t b}\right)\left[p\hat{A}_j(p) - pA_j(0)\right] \\ + \lambda_j^4\left[\lambda_j^2 + \frac{g}{b} + gY\right]\hat{A}_j(p) = 0.\end{aligned} \tag{14}$$

$A_j(0)$ is the sine Fourier transformation of the initial deflection of the sandwich beam given by the formula

$$w(x,0) = 4w_0\frac{x}{L}\left(1 - \frac{x}{L}\right). \tag{15}$$

According to (10)

$$A_j(0) = \frac{8w_0}{\lambda_j^3 L^2}\left[1 - (-1)^j\right]. \tag{16}$$

The decomposition into simple fractions allows to perform the inverse Laplace–Carson transformation. Finally, we obtained

$$A_j(t) = A_j(0)\frac{\sqrt{z}}{z}e^{-\frac{1}{2}\left(\beta q + \frac{c}{\mu}\right)t}\left[\left(\beta q + \frac{c}{\mu}\right)\sinh\frac{t}{2}\sqrt{z} + \sqrt{z}\cosh\frac{t}{2}\sqrt{z}\right], \tag{17}$$

where

$$q = \frac{gY\lambda_j^4 D_t b}{\mu\left(g + b\lambda_j^2\right)}, \tag{18}$$

$$z = \left(\beta q + \frac{c}{\mu}\right)^2 - 4\left(q + \frac{D_t\lambda_j^4}{\mu}\right). \tag{19}$$

For the solution (17) to be true in the current form, the following condition must be satisfied

$$z > 0. \tag{20}$$

Finally, according to (9) and (17) the transversal displacements w can be written in the following form

$$\begin{aligned}w(x,t) = \frac{2}{L}\sum_j A_j(0)\frac{\sqrt{z}}{z}e^{-\frac{1}{2}\left(\beta q + \frac{c}{\mu}\right)t}\left[\left(\beta q + \frac{c}{\mu}\right)\sinh\frac{t}{2}\sqrt{z} + \sqrt{z}\cosh\frac{t}{2}\sqrt{z}\right]\sin\lambda_j x \\ + w_f\tanh\alpha t.\end{aligned} \tag{21}$$

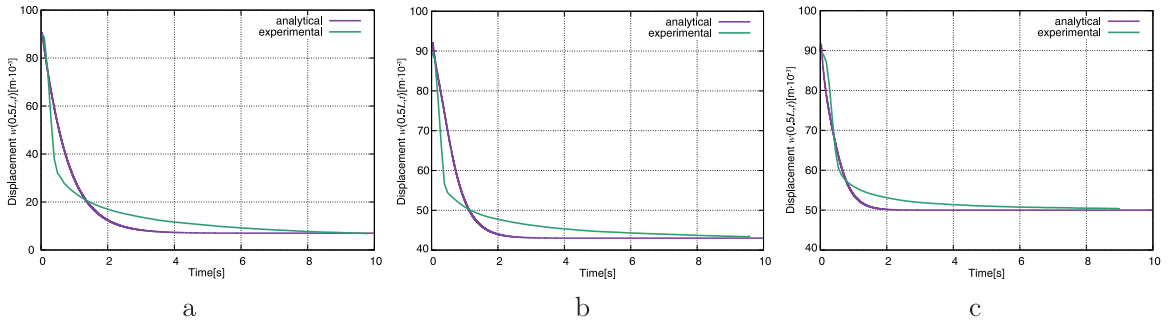

Fig. 10. Comparison of the displacements at the tip of the sandwich cantilever for initial displacement of 90 mm and: (a) no underpressure, (b) 0.04 MPa and (c) 0.08 MPa underpressure.

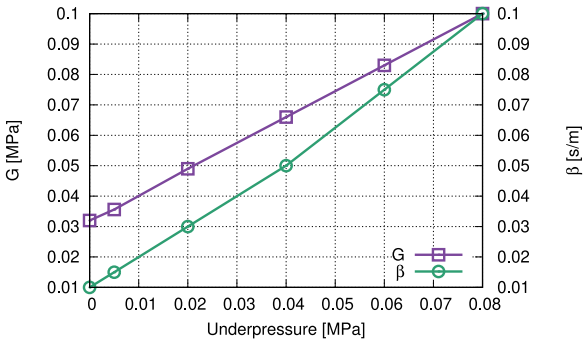

Fig. 11. Dependence of parameters G and β on underpressure.

The solution (21) was supplemented with a term responsible for reinforcing the sandwich beam. The presented mathematical model does not consider the phenomenon of friction between grains, which ultimately leads to blockage of the middle layer of the layered beam. Function $w_f \tanh \alpha t$ stabilises the solution at the level indicated by the parameter w_f, which is the final displacement of the beam. The α parameter is responsible for the reinforcement characteristics of the sand core.

The solution of the Eq. (21) with three terms of series compared with the experimental results is presented below. Parameters with the subscript "00" apply to the case without underpressure in the core, while the subscript "08" means underpressure in the core at the level of 0.08 MPa. The following set of data, consistent with the values used in the experiment, was used:

$$
\begin{array}{lll}
\mu = 0.842 \text{ kg/m}, & L = 1380 \text{ mm}, & E_1 = E_3 = 69 \times 10^3 \text{ MPa}, \\
b = 25 \text{ mm}, & h_2 = 15 \text{ mm}, & h_1 = h_3 = 2 \text{ mm}, \\
G_{00} = 0.032 \text{ MPa}, & G_{04} = 0.066 \text{ MPa}, & G_{08} = 0.10 \text{ MPa}, \\
\beta_{00} = 0.01 \text{ s/m}, & \beta_{04} = 0.05 \text{ s/m}, & \beta_{08} = 0.1 \text{ s/m}, \\
c = 100 \text{ kg/s/m}, & \alpha = 2.5 \text{ 1/s}. &
\end{array}
$$

A comparison between the experimental results and calculation results is shown in Fig. 10. The influence of underpressure on the shear stiffness G and the shear viscosity β is monotonic but not straight. Fig. 11 shows these dependencies, which were based on the analytical solution. The analytical responses were fitted to the experimental curves. Because only two parameters describe the rheological properties of the filling layer, the fitting of the analytical results is not perfect. There is a displacement discrepancy in the first stage of tip motion, which diminishes after several seconds.

Other initial deflections result in the exact coincidence of simulated displacements with experimental curves. The adjustment between analytical and experimental results is not perfect because the friction phenomenon between the grains in the core was not taken into account. Nevertheless, the obtained comparison shows that the analytical solution of the problem (21) depends only on a few parameters to describe the sandwich beam core with modified mechanical properties. The closed-form solution enables very fast calculations, which are especially favourable in complex optimisation. It also allows us to easily determine velocities and accelerations at any point of the beam. However, the obtained analytical solution is not general since of its undeniable limitations.

Although the above mathematical analysis is limited, it showed that a small number of material parameters is sufficient to describe the dynamics of a relatively complex task well. The mathematical model deviates from the physical model in the final stage of motion when the frictional jamming of the grains begins to dominate.

The following section will discuss the complex and simplified rheological beam model with a core filled with pressurised sand, which can be conveniently used for numerical simulations.

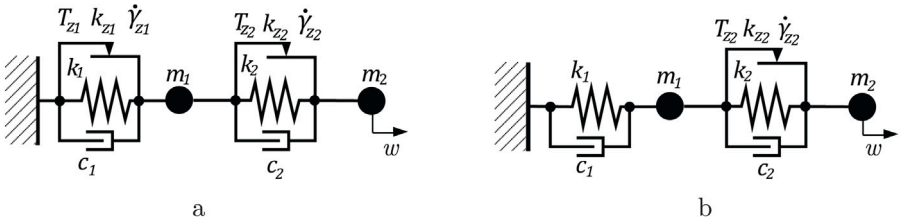

Fig. 12. Rheological model of a beam with a pressurised sand core: (a) full model with two frictional elements, and (b) simplified model with one frictional element.

6. Rheological model

The considered granular material exhibits non-classical properties because sand grains are suspended in a silicone polymer and compressed with underpressure, promoting agglomeration and sticking, while relative movements are small. The material properties tend to shift towards dense, viscous fluid.

A number of papers are devoted to the analysis and improvement of friction models for particular purposes, see for example the review paper [34] with a long list of references or [35,36], as well as a paper devoted to the identification of parameters [37,38]. In the academic literature, a generalised Maxwell model, models with a plastic flow without or with hardening, an elastic–viscoplastic and elastic with hardening-viscoplastic models are usually considered. Ultimately, the latter was chosen for further study. The frictional element is established with three parameters: the stick force limit T_z, hardening modulus k_z, and the flow rate coefficient denoted by $\dot{\gamma}_z$. The role of the model is to replicate the dynamics of such a complex system with a set of surrogate parameters, so neither the given parameters nor their values correspond to the physical parameters of the real sandwich beam.

The proposed rheological model consists of a pair of nonlinear oscillators with frictional elements connected in series (Fig. 12a). The task of two nonlinear frictional elements is to activate springs k_1 and k_2 along with the accompanying dashpots c_1 and c_2 at proper moments. Although a higher number of degrees of freedom would increase the fitting accuracy, a large number of parameters leads to an extensive computational effort. Identifying fewer parameters is favourable for introducing control strategies of switching underpressure between low (unjammed grains) and high value (jammed grains).

The force/displacement friction relation formulation uses the rate-independent perfect plasticity model. The total displacement is split into reversible elastic w_e and irreversible permanent w_f parts

$$w = w_e + w_f \ . \tag{22}$$

The force/displacement constitutive equation contains the coefficient of elastic stiffness k_z

$$F = k_z(w - w_f) \ . \tag{23}$$

The Coulomb friction law depends on the kinetic friction T_z

$$f(F, T_z) = |F| - T_z \ . \tag{24}$$

The motion equation is similar to the plastic flow $\dot{w}_p$

$$\dot{w}_p = \dot{\gamma} \ \mathrm{sign}(F) \ . \tag{25}$$

The loading and unloading conditions are

$$\dot{\gamma} = \begin{cases} 0 & \text{if} \quad f < 0, \\ \dot{\gamma}_0 & \text{if} \quad f = 0 \ \text{ and } \ \dot{f} = 0, \\ 0 & \text{if} \quad f = 0 \ \text{ and } \ \dot{f} < 0. \end{cases} \tag{26}$$

Practically, in numerical time-stepping simulation the equality condition is never fulfilled. The second condition in (26) is active when the friction flow function equals to zero in the intermediate time in the interval $[t, t_{i+1}]$. The full rheological model is described with 12 unknowns, combining nonlinear friction, springs, dashpots and masses, all of which depend on the underpressure value. Thus, the inverse problem that leads to minimisation of the norm of differences between the measured and computed response becomes significant. Consequently, it is necessary to reduce the number of parameters without harming the accuracy of the model. Identification and analysis of the variability of parameter values were performed to decide which parameters may be reduced, which may be assumed constant, and which depend heavily on the underpressure value.

The parameters of the simplified phenomenological model cannot be directly translated into the particular parameters of the physical system. The immanent feature of such a model is that specific rheological properties are combined, e.g. the internal damping of the metal face layers is merged with the core damping and some of the dissipation energy related to friction. These phenomena are combined in a single parameter c_2 and cannot be decomposed. In turn, the particular friction of the core material is described with parameters T_z and $\dot{\gamma}$, which both depend on the value of underpressure.

7. Identification

The experimental results for free vibration were conducted for five initial deflections u_0 and six underpressure values Δp from 0 to 0.08 MPa, so a total number of 30 curves representing displacement in time for each pair of values (u_0, Δp) were collected and used for identification.

The parameter identification of the rheological model, leading to the best possible agreement between the experimental and estimated response, can be achieved using either one of two approaches. In the first approach, the statistical analysis of multiply repeated measurements is traced. In the second, more meticulous approach, the identification procedure is based on the individual analysis of each of the experimental tests. The second approach was chosen to trace the variability of the model's parameters depending on the underpressure. It was anticipated that some parameters would be more vulnerable to underpressure, while others were expected to be less related.

When identifying parameters, the criterion of minimum difference between experimental and numerical displacements of the beam tip in time was assumed

$$I = \min\left(\max_{i=1..n} \|w_{\text{exp}} - w_{\text{num}}\|_2\right). \tag{27}$$

where n is the number of curves taken in simultaneous identification. The standard norm $\|\cdot\|_2$ was assumed as the measure of error in the entire time interval.

The evaluation takes a lot of computation effort and is quite time-consuming, but estimating the parameters over the entire catalogue of experimental results allowed to simplify the rheological model further. Selecting which of the estimated parameters can be assumed to be constant or even entirely removed allows us to establish a simplified model that would be more favourable for further optimisation of the damping control strategy.

Simplified models can conveniently replace realistic models requiring many parameters describing physical quantities. If some parameters having a similar influence on the response can be merged, adjusting the simplified model to the realistic one can be reasonable. In our case, these may be damping parameters describing dry or viscous friction or stiffness, as they directly rely on underpressure. On the other hand, these cannot be geometric parameters or inertia, as they are unrelated to underpressure changes.

The resulting parameters identification is depicted in Fig. 13, showing how the underpressure influences the decision variables under various initial conditions. The points for every abscissa as an applied underpressure value were determined for grouped five initial deflections. Index i in (27) runs over five experimental curves registered for various initial deflections of the free end at a single selected underpressure. We found that some of the values are less vulnerable to underpressure than others. The dashed lines show parameter distribution assumed after respective simplifications. We assumed that parameters that change from 0 to 1 would be considered the ones that were influencing the model more than parameters changing in a narrower range. The parameters that influence the system's response to a decisive extent are displayed in this case. Thus, $\dot{\gamma}_{z1}$ and T_{z2} that change from 0 to 1 were assumed to influence the model more than m_1 that changes from 0.6 to 0.2, and m_2 that changes from 0.18 to 0.22. Nevertheless, the masses m_1 and m_2 were assumed constant to stay faithful to physical limitations. The parameters responsible for dashpot damping c_1 and spring stiffness k_1 are close to constant zero, so they may be practically dismissed from the model. The flow rate coefficient $\dot{\gamma}_{z2}$ is also constantly close to zero. The second spring stiffness k_2, may be assumed as constant non-zero. Parameters such as k_{z1}, k_{z2}, c_2 and T_{z1} were also assumed as non-zero constants.

The remaining parameters, which are $\dot{\gamma}_{z1}$ and T_{z2}, highly depend on underpressure. They are close to 0 for no underpressure, and reach saturation for underpressure of 0.08 MPa. They were assumed as linearly dependent on the underpressure Δp.

Based on the results of the identification, the full model was simplified to a rheological model consisting of nine parameters, only two of which linearly depend on underpressure, namely: $\dot{\gamma}_{z1}$ and T_{z2}. Such a simplified model serves as a good feed for designing some advanced control strategy allowing to adjust underpressure to the type of dynamical load without performing multi-parameter time-consuming parametric optimisation. The simplified rheological model is presented in Fig. 12b. In this reduction, the number of parameters is decreased, but we do not necessarily remove those parameters that are equal to zero in Fig. 13. There are equivalent models that respond in the same way, although their schemes differ. This happens with both parallel and series connections. The parameters determined with the criterion (27) are listed below:

$$\begin{aligned} &k_{z_2} = 7.87 \text{ N/m}, && \dot{\gamma}_{z2} = 500{,}000 \text{ m}^2 \text{ s/kg} \cdot \Delta p + 25{,}000 \text{ m/s}, \; T_{z_2} = 1{,}250 \text{ m}^2 \cdot \Delta p + 100 \text{ N}, \\ &m_1 = 2.12 \text{ kg}, && m_2 = 29.85 \text{ kg}, \\ &k_1 = 4{,}909.90 \text{ N/m}, && k_2 = 3.97 \text{ N/m}, \\ &c_1 = 25.00 \text{ N s/m}, && c_2 = 135.66 \text{ N s/m} \end{aligned}$$

After such far-reaching reductions, the question is whether the simplified model properly mimics the non-linearity of the system.

The average relative error measure in the case of individual identification was lower than 0.0005. The biggest discrepancy is observed when exhibiting major dissipation at the initial stage of vibrations when the beam is released from deflection. At the first stage of the movement, the coupled oscillators in Fig. 12a are stiff and have low inertia m_1. The initial deflection induces quick relaxation of the potential energy related to parameter k_1, while spring k_2 is stretched because point 1 shifts back faster than point 2. After merely 0.35 s the second oscillator slowly relaxes, exhibiting high damping c_2 and notable frictional dissipation. In the model identified for five curves differing with initial deflections the same error measure reaches 0.002–0.02, i.e. can be expressed in a few percentages. For further determination of rheological parameters the assumed research method is correct.

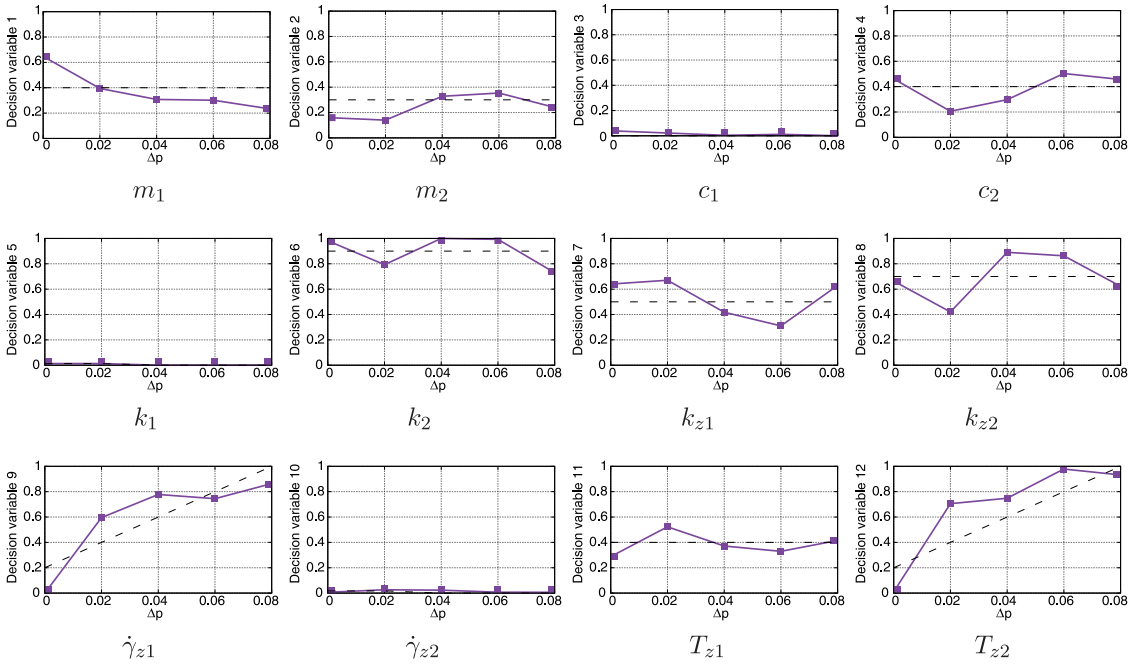

Fig. 13. Set of estimated decision variables of rheological model for different underpressure Δp.

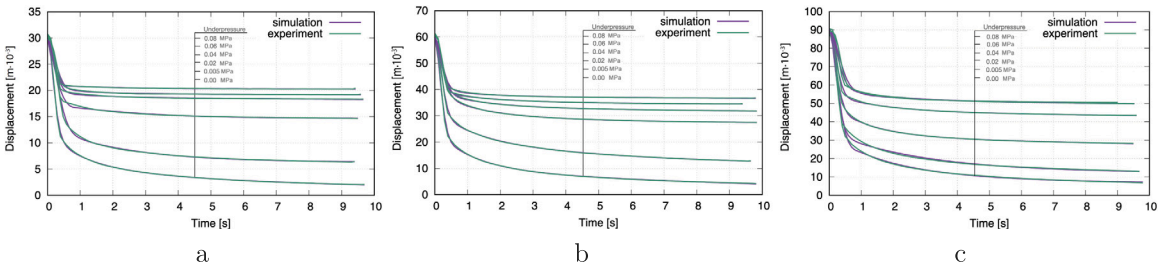

Fig. 14. Simulations compared with experimental results for various underpressure and initial deflections: (a) 30 mm, (b) 60 mm and (c) 90 mm.

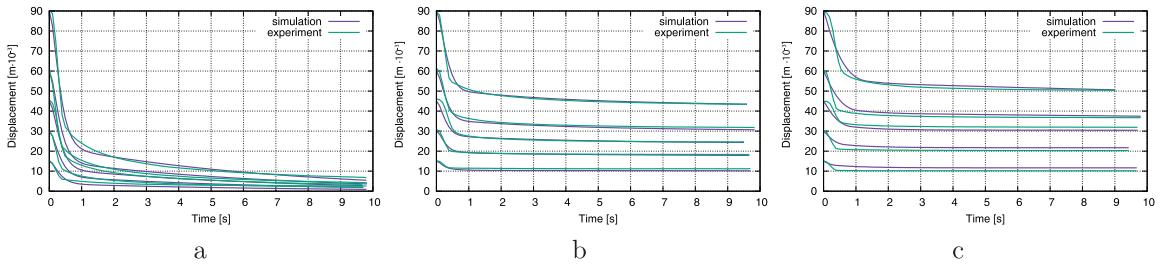

Fig. 15. Displacements in time for (a) no underpressure, (b) 0.04 MPa, (c) 0.08 MPa underpressure, and different initial deflection.

Fig. 14 presents a comparison of experimental results and the estimated curves for the simplified rheological model. The results of identification for different initial deflection shows that the simplified rheological model was capable of capturing the basic characteristic of the beam with a tunable core. The charts are consistent when displacement over time is considered for each of the selected initial deflections. When studying Fig. 15, one can see that for all cases of considered underpressure, no matter what deflection is imposed, the estimated results reasonably replicate the displacement over time. However, one has to notice that the stage of vibrations that is not accurately simulated is the initial stage at which the beam rapidly comes back to the equilibrium, and then sand grains start to heavily damp the vibrations. The exact moment of switching from high potential energy to high dissipation is less rapid during simulations, while the experimental result exhibits a sudden change.

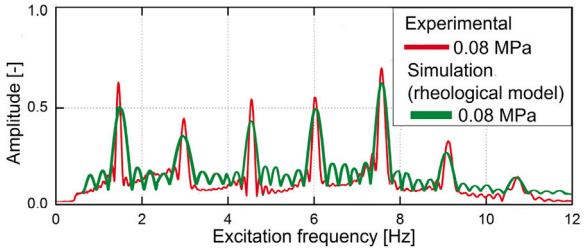

Fig. 16. Comparison of experimental and simulation results for different excitation frequencies.

One can notice a good agreement between the experimental and estimated results, showing that the simplified model can be used to accurately describe the system's dynamic, while being simple and consisting of only two pressure dependent parameters. The comparison of the experimental and simulation results obtained for the prescribed base motion show that the model captures well the shape of the maximum value of amplitude distribution and the maximum of the peak, which holds information about the damping properties of the system (Fig. 16). Nevertheless, the simulation results exhibit higher damping, demonstrating broader peaks for most tested frequencies.

8. Conclusions

Encapsulating dilatant sand in a special elastic envelope enables us to adjust the material's dissipating properties with a pneumatic control signal, resulting in an interesting and cost-effective alternative to smart materials.

The complex behaviour of the system can be fairly estimated with a mathematical model of a layered beam with a linearly viscoelastic core and shear stresses supplemented with a damping term, according to the Voigt model. The solution to the problem, supplemented with a term responsible for the pressure dependent reinforcement of the sand core, gave a fair agreement with the experimental results. The best agreement between the experimental and theoretical results was achieved for a twelve parameter rheological model of the system. Although accurate, the number of parameters to be identified and optimised makes this model less favourable. A relatively simple, nine parameter rheological model, with only two variables depending on underpressure, gives results one order worse than the full model. After identification, a set of two pressure-dependent parameters allowed good agreement between the model and the experimental results to be achieved, providing a fair amount of simplification while remaining faithful in describing the system's dynamics. Although the simplified model is less accurate, it is easier to adapt for further numerical optimisation problems.

The damping capacity of the system, using pressurised sand, may benefit from implementing a proper control strategies to release the strain energy accumulated during deformation, to achieve the ideal degree of vibration attenuation through the appropriate tuning of the underpressure control signal. This would allow for the efficient mitigation of vibration in structures subjected to dynamic excitation. Given that it has been proved experimentally, that it is plausible to use underpressure to adjust the properties of the dilatant sand to fit particular operating conditions, the identified parameters are relevant and indispensable for further study of control strategies for effective vibration abatement using the concept of switched jamming.

Declaration of competing interest

The authors declare the following financial interests/personal relationships which may be considered as potential competing interests: Czeslaw Bajer reports financial support was provided by Polish National Science Centre. Bartlomiej Dyniewicz reports financial support was provided by Polish National Science Centre.

Acknowledgements

This research has been supported within the projects UMO-2017/26/E/ST8/00532 and UMO-2019/33/B/ST8/02686 funded by the Polish National Science Centre, which is gratefully acknowledged by the authors.

References

[1] R. Zhang, H. Zhang, A. Zanoni, Q. Wang, P. Masarati, A tight coupling scheme for smooth/non-smooth multibody co-simulation of a particle damper, Mech. Mach. Theory 161 (2021) 104181.
[2] P. Veeramuthuvel, K.K. Sairajan, K. Shankar, Vibration suppression of printed circuit boards using an external particle damper, J. Sound Vib. 366 (2016) 98–116.
[3] X. Li, Y. Yang, W. Shi, Study on the damping effect of particle dampers considering different surface properties, Shock Vib. 2019 (2019) 8293654.
[4] J.M. Bajkowski, B. Dyniewicz, C.I. Bajer, Damping properties of a beam with vacuum-packed granular damper, J. Sound Vib. 341 (2015) 74–85.
[5] A.Q. Liua, B. Wang, Y.S. Choo, K.S. Ong, The effective design of bean bag as a vibroimpact damper, Shock Vib. 7 (2010) 343–354.
[6] M. Sanchez, G. Rosenthal, L.A. Pugnaloni, Universal response of optimal granular damping devices, J. Sound Vib. 331 (2012) 4389–4394.

[7] J.M. Bajkowski, B. Dyniewicz, C. Bajer, J. Bajkowski, An experimental study on granular dissipation for the vibration attenuation of skis, Proc. Inst. Mech. Eng. P J. Sports Eng. Technol. 235 (1) (2021) 13–20.
[8] C. Saluena, T. Poschel, S.E. Espiov, Dissipative properties of granular materials, Phys. Rev. E 59 (1999) 4422–4425.
[9] M.A. Aguirre, N. Nerone, I. Ippolito, A. Calvo, D. Bideau, Granular packing: influence of different parameters on its stability, Granul. Matter 2 (1) (2001) 75–77.
[10] B. Chakraborty, R.P. Behringer, Jamming of granular matter, Encycl. Complex. Syst. Sci. 4697 (2009) 4997–5021.
[11] L. Gagnon, M. Morandini, G.L. Ghiringhelli, A review of particle damping modeling and testing, J. Sound Vib. 459 (2019) 114865.
[12] J. de Vicente, D.J. Klingenberg, R. Hidalgo-Alvarez, Magnetorheological fluids: a review, Soft Matter 7 (2011) 3701–3710.
[13] A.S. Semisalova, N.S. Perov, G.V. Stepanov, E. Kramarenko, A.R. Khokhlov, Strong magnetodielectric effects in magnetorheological elastomers, Soft Matter 9 (2013) 11318–11324.
[14] A.O. Ozer, Modeling and control results for an active constrained layered (ACL) beam actuated by two voltage sources with/without magnetic effects, IEEE Trans. Automat. Control 62 (12) (2017) 6445–6450.
[15] T. Hesse, M. Ghorashi, D. Inman, Shape memory alloy in tension and compression and its application as clamping-force actuator in a bolted joint: Part 1 — experimentation, J. Intell. Mater. Syst. Struct. 15 (2004) 577–587.
[16] C.X. Wong, J.A. Rongong, Control of particle damper nonlinearity, AIAA J. 47 (4) (2009) 953–960.
[17] N. Tang, J.A. Rongong, N. Sims, Design of adjustable tuned mass dampers using elastomeric o-rings, J. Sound Vib. 433 (2018) 334–348.
[18] J.A. Rongong, G.R. Tomlinson, Amplitude dependent behaviour in the application of particle dampers to vibrating structures, in: 46th AIAA/ASME Structures, Structural Dynamics and Materials Conference, Austin, Texas, 2005, pp. 1–9.
[19] A.J. Loeve, O.S. Van de Ven, J.G. Vogel, P. Breedveld, J. Dankelmann, Vacuum packed particles as flexible endoscope guides with controllable rigidity, Granul. Matter 12 (6) (2010) 543–554.
[20] E. Brown, N. Rodenberg, J. Amend, A. Mozeika, E. Steltz, M.R. Zakin, H. Lipson, H.M. Jaeger, Universal robotic gripper based on the jamming of granular material, Proc. Natl. Acad. Sci. USA 107 (44) (2010) 18809–18814.
[21] J.M. Bajkowski, R. Zalewski, Transient response analysis of a steel beam with vacuum packed particles, Mech. Res. Commun. 60 (2014) 1–6.
[22] D. Rodak, R. Zalewski, Innovative controllable torsional damper based on vacuum packed particles, Materials 13 (19) (2020).
[23] G.H. Ristow, Critical exponents for granular phase transitions, Europhys. Lett. 40 (6) (1997) 625–630.
[24] A. Jiang, A. Ataollahi, K. Althoefer, P. Dasgupta, A variable stiffness joint by granular jamming, in: Proc. of ASME IDETC and CIE Conference, Chicago, IL, 2012, pp. 1–9.
[25] M. Botom, E. Azema, N. Estrada, F. Radjai, A. Lizcano, Quasi-static rheology of granular packings composed of platy clay-like particles, Phys. Rev. E 87 (2013) 032206.
[26] M.E. Cates, J.P. Wittmer, J.P. Bouchaud, P. Claudin, Jamming, force chains, and fragile matter, Phys. Rev. Lett. 81 (1998) 1841–1844.
[27] E. Kausel, D. Assimaki, Seismic simulation of inelastic soils via frequency-dependent moduli and damping, J. Eng. Mech. 128 (1) (2002) 34–47.
[28] N. Delepine, L. Lenti, G. Bonnet, J.-F. Semblat, Nonlinear viscoelastic wave propagation: An extension of nearly constant attenuation models, J. Eng. Mech. 135 (11) (2009) 1305–1314.
[29] D.R. Groholski, Y.M.A. Hashash, B. Kim, M. Musgrove, J. Harmon, J.P. Stewart, Simplified model for small-strain nonlinearity and strength in 1D seismic site response analysis, J. Geotech. Geoenviron. Eng. 142 (9) (2016) 04016042.
[30] N. Gerolymos, G. Gazetas, Constitutive model for 1-D cyclic soil behaviour applied to seismic analysis of layered deposits, Soils Found. 45 (3) (2005) 147–159.
[31] A. Pain, S. Nimbalkar, M. Hussain, Applicability of Bouc-Wen model to capture asymmetric behavior of sand at high cyclic shear strain, Int. J. Geomech. 20 (6) (2020) 06020009.
[32] P. Bartkowski, R. Zalewski, P. Chodkiewicz, Parameter identification of Bouc-Wen model for vacuum packed particles based on genetic algorithm, Arch. Civ. Mech. Eng. 19 (2) (2019) 322–333.
[33] D.J. Mead, S. Markus, The forced vibration of a three-layer, damped sandwich beam with arbitrary boundary conditions, J. Sound Vib. 10 (2) (1969) 163–175.
[34] E.J. Berger, Friction modeling for dynamic system simulation, Appl. Mech. Rev. 55 (6) (2002) 535–577.
[35] W.G. Sawyer, N. Argibay, D.L. Burris, B.A. Krick, Mechanistic studies in friction and wear of bulk materials, Annu. Rev. Mater. Res. 44 (1) (2014) 395–427.
[36] Y.F. Liu, J. Li, Z.M. Zhang, X.H. Hu, W.J. Zhang, Experimental comparison of five friction models on the same test-bed of the micro stick–slip motion system, Mech. Sci 6 (2015) 15–28.
[37] D.D. Rizos, S.D. Fassois, Presliding friction identification based upon the Maxwell slip model structure, Chaos 14 (2) (2004) 431–445.
[38] B.M. Nouri, Friction identification in mechatronic systems, ISA Trans. 43 (2) (2004) 205–216.